
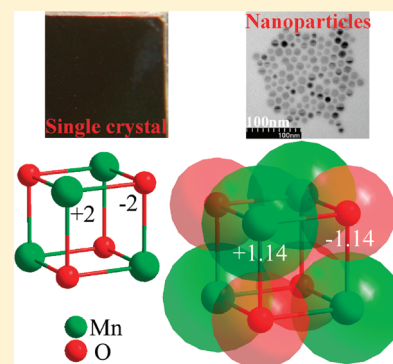


Experimental Determination of Ionicity in MnO Nanoparticles

Qi -C. Sun,[†] Xiaoshan Xu,^{S,†} Sheila N. Baker,^{¶,‡} Andrew D. Christianson,[‡] and Janice L. Musfeldt^{*,†}[†]Department of Chemistry, University of Tennessee, Knoxville, Tennessee 37996, United States[‡]Neutron Scattering Science Division, Oak Ridge National Laboratory, Oak Ridge, Tennessee 37831, United States Supporting Information

ABSTRACT: Phonons are exquisitely sensitive to finite-length scale effects in complex materials because they are intimately connected to charge, polarizability, and structure, and a quantitative analysis of their behavior can reveal microscopic aspects of chemical bonding. To investigate these effects in a model correlated oxide, we measured the infrared vibrational properties of 8-nm particles of MnO, compared the results with the analogous bulk material, and quantified the phonon confinement with a calculation of the Born effective charge. Our analysis reveals that the Born effective charge decreases by ~20%, compared to the bulk material. Moreover, this change impacts both ionicity and polarizability. Specifically, we find that MnO nanoparticles are ~12% less ionic than the corresponding bulk. This discovery is important for understanding finite-length scale effects in this simple binary oxide and the more complicated functional oxides that emanate from this parent compound.

KEYWORDS: MnO, nanoparticles, phonon confinement, Born effective charge, finite length scale effect, ionicity



■ INTRODUCTION

The interplay between charge and structure governs the properties of many complex oxides, including superconductors, thermoelectrics, and multiferroics.^{1–4} However, less is known about strain and finite-length scale effects. One challenge is understanding exactly how the microscopic aspects of chemical bonding should be quantified in nanomaterials. Fundamental physical quantities such as the Born effective charge can,⁵ for instance, reveal essential aspects of charge, strain, and bonding.^{6,7} This is because the Born effective charge contains both local and nonlocal contributions that are represented by local effective charge and total polarizability (see Figure 1). To test these ideas, we elected to work with MnO, which is a chemically and structurally simple salt for which both bulk and nanoscale analogs are available. Our selection of MnO was further motivated by the fact that this binary oxide is the parent compound for many functional materials, such as colossal magnetoresistant manganites,⁸ making evaluation of size effects highly attractive.

Bulk MnO displays a $Fm\bar{3}m$ rocksalt structure with a lattice constant of 4.4448 Å at 300 K.⁹ Group theory predicts only one triply degenerate infrared active vibration mode.¹⁰ Previous infrared investigations focused on the analysis of the Reststrahlen band, its anharmonic character, and evaluation of the Born and local (Szigeti) effective charges for the Mn center ($Z_B^* = 2.2$ – 2.6 e , $Z^* = 1.08$ e).^{11–16} Here, e is the electronic charge. These literature values show that, even in a highly ionic material like MnO, the system is far from the Madelung limit. The discovery of nanoscale MnO enables investigation of finite-length scale effects.^{17–21} Major findings at this time include synthetic techniques that yield excellent size/shape control and the possibility of ferromagnetism (or an uncompensated ferromagnetic surface) at small particle sizes.^{17–21}

To further investigate finite-length scale effects in model transition-metal oxides, we measured the infrared vibrational properties of nanoscale MnO, compared the results with the analogous bulk material, and quantified the phonon confinement with a calculation of the Born effective charge. Our analysis reveals that the Born effective charge decreases by ~20% in 8-nm nanoparticles at 300 K, which is a reduction that can be separated into total polarizability and local effective charge contributions. Changes in the latter show that MnO nanoparticles are ~12% less ionic than the extended solid. These differences, illustrated here for a simple binary metal oxide, provide foundational understanding of the interplay between charge and structure in confined systems that may have parallels in other functional oxides.^{22–24}

■ MATERIALS AND METHODS

MnO nanoparticles were synthesized using a manganese–myristic acid salt combined with an additional activating/directing agent in 1-octadecene, as detailed in the Supporting Information. The mixture was heated to 305 °C to yield almost-monodisperse particles.²⁵ The average particle diameter estimated from transmission electron microscopy (TEM) is 8 ± 1.8 nm (see Figure 2c), which is consistent with that obtained from X-ray diffraction. Our growth process was not able to produce a wide variety of sizes. X-ray diffraction confirms the presence of a single cubic phase. The nanoparticles are essentially isostructural with the bulk within our sensitivity.²⁶ Thermogravimetric analysis indicates that the myristic acid capping ligand

Received: February 24, 2011

Revised: April 22, 2011

Published: May 12, 2011

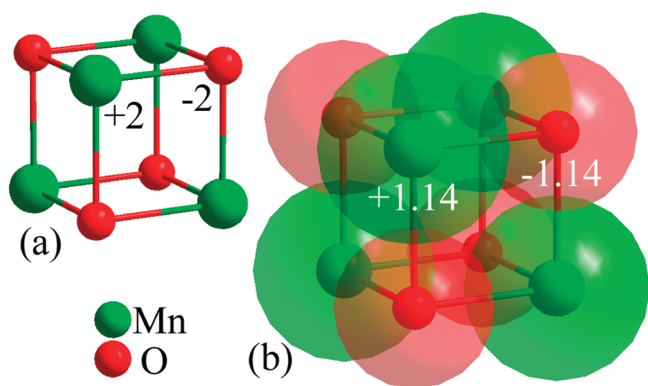


Figure 1. (a) Schematic view of an ideal ionic crystal of MnO composed of divalent cations and divalent anions. (b) Schematic view of a more-realistic MnO crystal that is away from the Madelung limit. Here, local effective charge (ionicity) is given by +1.14 and −1.14. The transparent regimes schematically indicate electron clouds (total polarizability) that are shared by the involved atoms, with electron density concentrated in the regions between atomic centers. The Born effective charge includes the combined effects of the local effective charge and total polarizability.

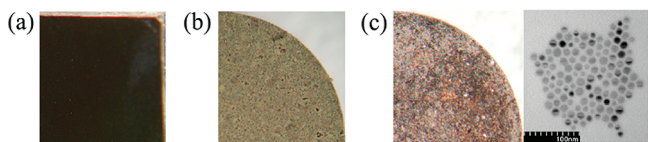


Figure 2. Photographs of (a) the single-crystal surface and (b) the bulk powder pellet surface. (c) Right: photograph of the nanoparticle pellet surface. Left: TEM image of 8 ± 1.8 nm nanoparticles (the scale bar is 100 nm).

comprises $\sim 25\%$ of the total sample mass. This capping ligand stabilizes the large uncompensated surface. For comparison, a well-polished (100)-oriented MnO single crystal and MnO bulk powder (99.99+) were purchased directly from Princeton Scientific and Sigma Aldrich, respectively. The average particle diameter in the bulk powder was 0.25 mm. Pressed pellets of nanoscale and bulk powder MnO were prepared in order to investigate their dynamical properties. Pellet densities are $\sim 47\%$ and $\sim 74\%$ of the single-crystal density.²⁷ Figure 2 displays photographs of all sample surfaces. As expected, the highly polished single crystal (Figure 2a) is of optical quality, whereas surface roughness effects are evident in the bulk powder (Figure 2b) and nanoparticle (left-hand image, Figure 2c) pellets. The right-hand side of Figure 2c shows a TEM image of 8-nm nanoparticles.

Near-normal infrared reflectance was measured using a series of spectrometers, including a Bruker Model 113 V Fourier transform infrared spectrometer, an Equinox 55 Fourier transform instrument (equipped with a microscope attachment), and a Perkin–Elmer Model Lambda 900 grating spectrometer, covering the frequency range from 25–52 000 cm^{-1} . A helium-cooled bolometer detector was employed in the far-infrared for added sensitivity. A resolution of 2 cm^{-1} was used in the infrared region, whereas a resolution of 3 nm was employed in the optical regime. As mentioned above, surface roughness effects are important for both the bulk powder and nanoparticle pellets. A 2000 Å aluminum overcoat was used to correct for the associated scattering effects.²⁸ We also sought to account for the spectral contribution of the capping ligand in the nanoparticle response.²⁹ This was

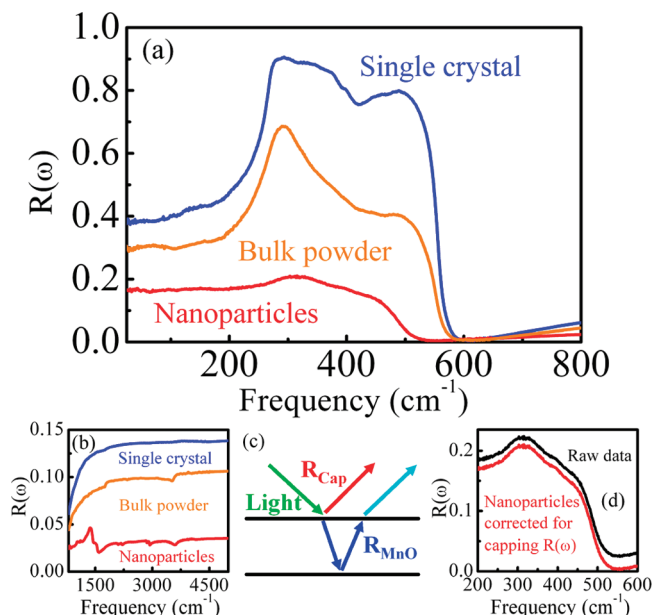


Figure 3. (a) Far-infrared reflectance spectra of single-crystal, bulk powder, and nanoscale MnO, corrected for surface scattering and capping ligand reflectance, at 300 K. (b) Middle-infrared spectra of single-crystal, powdered, and 8-nm MnO. (c) Schematic diagram of the two-layer assumption. (d) Effect of the two-layer correction on the reflectance of nanoscale MnO.

done with a traditional two-layer multiple reflectance model,³⁰ shown schematically in Figure 3c.³¹ Combining the various reflectance and transmittance processes, we can express the reflectance of nanoscale MnO as $R_{\text{MnO}} = (R_{\text{Meas}} - R_{\text{Cap}})/(1 - 2R_{\text{Cap}} + R_{\text{Cap}}R_{\text{Meas}})$. Here, R_{MnO} is the corrected reflectance of nanoscale MnO, R_{Cap} is the reflectance of capping ligands in isolation (assumed to be constant at 0.022, which is a reasonable value for an organic), and R_{Meas} is the measured reflectance. Figure 3d shows a comparison of the measured and corrected reflectance of the nanoparticles. The net effect is to shift the reflectance to give a better-defined plasma edge. The various capping ligand, density, and scattering modifications are summarized in Table 1.

In this work, we employed a Kramers–Kronig analysis to calculate the optical constants of single-crystal, bulk powder, and nanoscale MnO.^{32,33} The advantage of this procedure is that it directly relates reflectance and phase shift to the complex dielectric response of a material: $\epsilon(\omega) = \epsilon_1(\omega) + i\epsilon_2(\omega) = \epsilon_1 + (4\pi i/\omega)\sigma_1(\omega)$, where $\sigma_1(\omega)$ is the optical conductivity.^{32,33} A partial sum rule analysis of the optical conductivity thus allowed us to extract an effective plasma frequency (ω_p), and the value of the effective high-frequency dielectric constant ($\epsilon_1(\infty)$), which can be obtained from appropriate limit of $\epsilon_1(\omega)$. One more step is required to get the intrinsic optical constants. The intrinsic value of the effective plasma frequency ω_p' is related to the ω_p value extracted from a Kramers–Kronig analysis as $\omega_p'^2 = (\omega_p')^2 \nu$.^{34,35} Similarly, the intrinsic value of the effective high-frequency dielectric constant $\epsilon_1'(\infty)$ is related to the extracted value: $\epsilon_1(\infty) = 1 + [\epsilon_1'(\infty) - 1]\nu$.^{34,35} Here, ν is the scaling factor. In our implementation, it refers to the combination of pellet density and amount of MnO in the sample. Thus, for the bulk powder, $\nu = 0.74$. For the nanoparticles, $\nu = (0.47) \cdot (0.75)$, a combination of density and surface coverage

Table 1. Summary of the Sample and Spectral Corrections Used in This Work

correction	single crystal	bulk powder	nanoparticles
surface scattering		aluminum overcoat	aluminum overcoat
capping ligand reflectance			two-layer model
pellet density effects		density scaling factor ≈ 0.74	density scaling factor $\approx 0.47^a$
quantity of capping ligand			thermogravimetric analysis
			$x_{\text{Cap}} \approx 0.25$, $x_{\text{MnO}} \approx 0.75^b$

^a This is the density relative to that of the single crystal. ^b The mass fractions x_{Cap} and x_{MnO} account for the relative quantity of myseric acid ligand and MnO, respectively, in the sample.

effects. Of course, $\nu = 1.0$ for the single crystal. The rationale for this analysis is summarized in Table 1. We note that density corrections were successfully employed in the MoS₂ system.³⁴ The intrinsic values of $(\omega'_p)^2$ and $\epsilon'_1(\infty)$ are obtained by this procedure and shown in Table 2.

RESULTS AND DISCUSSION

Figure 3a displays the infrared reflectance of single-crystal, bulk powder, and nanoscale MnO at 300 K. There is one vibrational mode, in agreement with group theoretical predictions. As anticipated,^{11,13,14,36} the spectrum is broad and shows strong anharmonic effects, similar to other simple salts such as NaCl and KBr.^{37,38} Therefore, our approach to the investigation of charge and bonding in bulk and nanoscale MnO consists of (i) a measurement of reflectance (Figure 3),³⁶ (ii) subsequent calculation of optical conductivity via a Kramers–Kronig analysis (Figure 4), (iii) extraction of the oscillator strength or plasma frequency and application of appropriate corrections for density and capping ligand effects (as detailed in the Methods section) to yield the intrinsic optical constants, and (iv) an effective charge analysis.

Table 2 summarizes the intrinsic values of the squared effective plasma frequency and high-frequency dielectric constant for single-crystal, bulk powder, and nanoscale MnO. The values obtained for both bulk materials agree well with each other and similar data in refs 11, 13, and 14. Small size reduces $(\omega'_p)^2$ from 12.26×10^5 to $7.74 \times 10^5 \text{ cm}^{-2}$. $\epsilon'_1(\infty)$ is reduced from 4.82 to 4.21. Based on these intrinsic optical constants, we can calculate the effective charge, according to the rigid ion model.^{6,7,34} The latter gives a precise relationship between the effective plasma frequency and the Born effective charge:

$$4\pi^2 c^2 \sum_j (\omega'_{p,j})^2 = 4\pi^2 c^2 \epsilon'_1(\infty) \sum_j ((\omega'_{\text{LO},j})^2 - (\omega'_{\text{TO},j})^2) = \frac{Ne^2}{\epsilon_0 V} \sum_k \frac{(Z_{\text{B},k}^*)^2}{m_k} \quad (1)$$

Here, $Z_{\text{B},k}^*$ is the Born effective charge on the k th ion; $\omega'_{p,j}$ is the intrinsic value of the effective plasma frequency for the j th oscillator; ω'_{TO} and ω'_{LO} are the intrinsic transverse and longitudinal optical phonon frequencies, respectively; $\epsilon'_1(\infty)$ is the intrinsic effective high-frequency dielectric constant; N is the number of formula units in the unit cell; V is the volume of the MnO formula unit; m_k is the atomic mass of the k th atom; ϵ_0 is the permittivity of free space; e is the electronic charge; and c is the speed of light. The sum rule, $\sum Z_{\text{B},k}^* = 0$, guarantees that the charge neutrality condition is fulfilled. This rendering is well-suited to the analysis of both bulk and nanomaterials,^{34,35} and is employed in this work to evaluate charge and bonding in MnO.

Table 2. Optical Constants of Single Crystal, Bulk Powder, and Nanoscale MnO as Extracted from the Measured Reflectance Spectrum by an Kramers–Kronig Analysis, Along with the Born (Z_{B}^*) and Local (Z^*) Effective Charge for the Mn Center, and Total Polarizability (α)^a

material	$(\omega'_p)^2 (\times 10^5 \text{ cm}^{-2})$	$\epsilon'_1(\infty)$	$Z_{\text{B}}^* (e)$	$\alpha (\text{\AA}^3)$	$Z^* (e)$
single crystal	12.26	4.82	2.60	36.9	1.14
bulk powder	11.54	4.85	2.53	37.0	1.11
nanoparticles	7.74	4.21	2.06	34.0	1.00
difference			−20%	−8%	−12%

^a Detailed error bar information is provided in ref 40. The total polarizability (α) is the sum of the cationic and anionic polarizabilities.

Table 2 displays the Born effective charge, Z_{B}^* , for the Mn center of single crystalline, bulk powder, and nanoscale MnO, calculated according to eq 1. Within our sensitivity, the Born effective charge of the single-crystal and bulk powder are almost identical ($Z_{\text{B}}^* = 2.60 e$ vs $2.53 e$), as they should be, once density is taken into account.³⁹ This correspondence demonstrates that the approach outlined here can be reliably extended to analyze powdered materials.^{34,35} The results are also consistent with previous estimates of Z_{B}^* in bulk MnO.^{15,16}

This analysis also reveals striking finite-size effects. Compared to the chemically identical but morphologically different bulk material, the Born effective charge of the nanoparticles is reduced significantly, by $\sim 20\%$ (from $2.60 e$ to $2.06 e$). Similar effects were observed in the intralayer direction of the model transition metal dichalcogenide MoS₂, where Z_{B}^* of the Mo center drops from $1.11 e$ in the bulk material to $0.69 e$ in the nested nanoparticles.³⁴ In order to understand this trend, it is useful to realize that Z_{B}^* contains both dynamic and static contributions. Decomposition is needed to quantify the impact of confinement on charge and bonding. Total polarizability (α) and local effective charge (Z^*) are given as^{34,35}

$$\alpha = \frac{V \cdot (\epsilon'_1(\infty) - 1)}{N \cdot (n\epsilon'_1(\infty) - n + 1)} \quad (2a)$$

$$Z^* = Z_{\text{B}}^* \left[1 - n \left(\frac{N\alpha}{V} \right) \right] \quad (2b)$$

Here, n is the depolarization factor.⁴¹ N and V are defined as previously described. In this rendering, α is the sum of cationic and anionic contributions. From the physical point of view, polarizability is proportional to the electron cloud volume. Changes in α measure electron cloud distortion and are

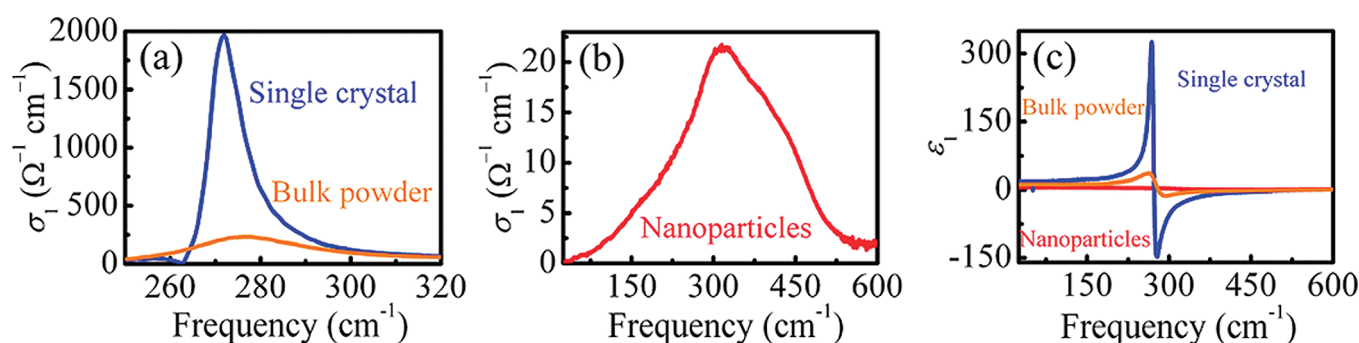


Figure 4. (a) Optical conductivity of single-crystal and bulk powder MnO at 300 K. (b) Conductivity of nanoscale MnO at 300 K. (c) ϵ_1 of single-crystal, bulk powder, and nanoscale MnO. The extremely broad peak in $\sigma_1(\omega)$ of the nanoparticles indicates a much shorter phonon lifetime, compared to the bulk, which does not impact the value of Z_B^* .

long-range effects. The local effective charge is different. It is, by nature, a short-range interaction related to relative ionic displacement and quantifies chemical bonding. For a fully covalent material such as diamond or silicon, $Z^* \approx 0$ e, whereas for a strongly ionic compound such as NaCl, $Z^* = 0.8$ e for the Na site.⁴² Previous estimates place the local effective charge of bulk MnO at 1.08 e for the Mn center.¹³ This framework, along with the vibrational response of bulk and nanoscale MnO (Figure 3), can be used to quantify finite-size effects on the total polarizability and the local effective charge.

Table 2 displays the total polarizability and local effective charge for single-crystal, bulk powder, and nanoscale MnO at room temperature, calculated according to eqs 2a and 2b. Our estimate of Z^* for the Mn center in bulk MnO (both single-crystal and bulk powder) is in excellent agreement with that in ref 13. The findings for the nanoparticles are quite different. Our analysis reveals that the total polarizability decreases by $\sim 8\%$ in the nanoparticles, whereas local effective charge (or ionicity) decreases by $\sim 12\%$. The fact that nanoscale size effects in MnO manifest themselves in both α and Z^* is fundamentally different than the situation in MoS_2 , where the confinement that acts to reduce Born effective charge in the nested nanoparticles is fully contained in the total polarizability.³⁴ How should we interpret these changes in MnO? One immediate and very accessible finding is that the 8-nm nanoparticles are less ionic than the bulk material, as evidenced by the decrease in Z^* from 1.14 e to 1.00 e (see Table 2). This can be viewed as a finite-size-induced change in oxidation state. It does not seem to be an “expanded volume effect” within the nanoparticles, because the lattice constants of bulk and nanoscale MnO are almost identical within our sensitivity.²⁶ Interpreted in terms of improved electron cloud overlap (which favors stronger covalent interactions),⁴³ the reduced total polarizability of the MnO nanoparticles reinforces the ionicity trend. Taken together, the decrease in both α and Z^* in the 8-nm MnO nanoparticles reveals modified interactions that stabilize the large uncompensated surface and balance the associated strain.

It is interesting to consider exactly where this charge deficiency might reside in the 8-nm MnO nanoparticles. [Here, the phrase “charge deficiency” refers to the reduced chemical bond ionicity, not free-standing charge.] Infrared spectroscopy is a microscopic technique, but, similar to many other physical probes, the spatial resolution is wavelength-limited and, as such, provides a spatial (ensemble) average. Therefore, the aforementioned effective charges and total polarizability are average

quantities (i.e., on average, the MnO nanoparticles are $\sim 12\%$ less ionic than the extended solid). While our experiments do not reveal precisely how charge is distributed in a nanoparticle, several limiting cases can be considered. For instance, (i) charge can be preferentially localized in the outer layers, with pinning due to strain and the uncompensated surface; (ii) charge may be homogeneously distributed over the entire 8-nm nanoparticle; and (iii) charge can be inhomogeneously distributed over the particle with a length scale that describes relaxation of charge and strain, given by the dielectric and elastic characteristics of the material. Because of surface strain and capping ligand–uncompensated surface interactions, the lattice of the nanoparticle sample will respond less readily than that of the single crystal to outside stimuli. This suggests that the reduced ionicity or “charge deficiency” may preferentially localize in the surface layers. However, there is certainly no skin effect in a dielectric. A reasonable compromise is to allow the charge deficiency and associated lattice distortion to disappear gradually. Consideration of a simple dielectric sphere provides insight here and suggests a relevant length scale of a few unit cells,⁴⁴ analogous to polar surface reconstruction, which is well-known to lower ionicity.⁴⁵

CONCLUSIONS

To summarize, the dynamical properties of a material are exquisitely sensitive to the interplay between charge and structure. We exploit this sensitivity to evaluate finite-length scale effects in the nanoscale analogue of a model correlated oxide, MnO, using the Born and local effective charge to quantify chemical bonding. This analysis reveals a dramatic decrease in the Born effective charge of the nanoparticles, compared with the bulk material, which is a finding that, when separated into local effective charge and total polarizability contributions, shows that the nanoparticles are less ionic than bulk MnO. The latter can be viewed as a finite-size-induced change in oxidation state. These findings are important for understanding finite-length scale effects in this simple binary oxide and the more-complicated functional oxides that emanate from this parent compound. They are also useful for the development of nanoscale electronic devices.

ASSOCIATED CONTENT

S Supporting Information. Experimental procedures, elemental characterization, and additional images. (PDF) This information is available free of charge via the Internet at <http://pubs.acs.org>.

AUTHOR INFORMATION

Corresponding Author

*E-mail: musfeldt@utk.edu.

Present Addresses

⁵Oak Ridge National Laboratory, Oak Ridge, TN 37831, USA.

[†]Department of Chemical Engineering, University of Missouri—Columbia, Columbia, MO 65211, USA.

ACKNOWLEDGMENT

Research at UT was supported by the Joint Directed Research and Development Program and the JIAM Seed Program at the University of Tennessee, along with the Materials Science Division, Basic Energy Sciences, U.S. Department of Energy (Contract No. DE-FG02-01ER45885). Work at ORNL was supported by the Laboratory Directed Research and Development Program of Oak Ridge National Laboratory, managed by UT-Battelle, LLC, for the U.S. Department of Energy. We thank Dr. C. H. Wang and Prof. M. -H. Whangbo for useful discussions.

REFERENCES

- Orenstein, J.; Millis, A. J. *Science* **2000**, 288, 468–474.
- Cheong, S.-W.; Mostovoy, M. *Nat. Mater.* **2007**, 6, 13–20.
- Dresselhaus, M. S.; Chen, G.; Tang, M. Y.; Yang, R.; Lee, H.; Wang, D.; Ren, Z.; Fleurial, J.-P.; Gogna, P. *Adv. Mater.* **2007**, 19, 1–12.
- Navrotsky, A.; Ma, C.; Lilova, K.; Birkner, N. *Science* **2010**, 330, 199–201.
- Born, M.; Huang, K. *Dynamical Theory of Crystal Lattices*; Oxford University Press: London, 1954.
- Resta, R.; Posternak, M.; Baldereschi, A. *Phys. Rev. Lett.* **1993**, 70, 1010–1013.
- Homes, C. C.; Vogt, T.; Shapiro, S. M.; Wakimoto, S.; Ramirez, A. P. *Science* **2001**, 293, 673–676.
- Dagotto, E. *Nanoscale Phase Separation and Colossal Magnetoresistance: The Physics of Manganites and Related Compounds*; Springer: Berlin, 2003.
- Wyckoff, R. W. G. *Crystal Structures*; Interscience: New York, 1963.
- Haywood, B. C.; Collins, M. F. J. *Phys. C: Solid State Phys.* **1971**, 4, 1299–1305.
- Rudolf, T.; Kant, Ch.; Mayr, F.; Loidl, A. *Phys. Rev. B* **2008**, 77, 024421.
- Charges on the O centers are obviously equal and opposite.
- Plendl, J. N.; Mansur, L. C.; Mitra, S. S.; Chang, I. F. *Solid State Commun.* **1969**, 7, 109–111.
- Mochizuki, S. J. *Phys.: Condens. Matter* **1989**, 1, 10351–10359.
- Savrasov, S. Y.; Kotliar, G. *Phys. Rev. Lett.* **2003**, 90, 056401.
- Wdowik, U. D.; Legut, D. J. *Phys.: Condens. Matter* **2009**, 21, 275402.
- Lee, G. H.; Huh, S. H.; Jeong, J. W.; Choi, B. J.; Kim, S. H.; Ri, H.-C. *J. Am. Chem. Soc.* **2002**, 124, 12094–12095.
- Seo, W. S.; Jo, H. H.; Lee, K.; Kim, B.; Oh, S. J.; Park, J. T. *Angew. Chem., Int. Ed.* **2004**, 43, 1115–1117.
- Ghosh, M.; Biswas, K.; Sundaresana, A.; Rao, C. N. R. *J. Mater. Chem.* **2006**, 16, 106–111.
- Morales, M. A.; Skomski, R.; Fritz, S.; Shelburne, G.; Shield, J. E.; Yin, M.; O'Brien, S.; Leslie-Pelecky, D. L. *Phys. Rev. B* **2007**, 75, 134423.
- Schladt, T. D.; Graf, T.; Tremel, W. *Chem. Mater.* **2009**, 21, 3183–3190.
- Cao, J.; Vergara, L. I.; Musfeldt, J. L.; Litvinchuk, A. P.; Wang, Y. J.; Park, S.; Cheong, S. W. *Phys. Rev. Lett.* **2008**, 100, 1772051.
- Kim, M.; Chen, X. M.; Joe, Y. I.; Fradkin, E.; Abbamonte, P.; Cooper, S. L. *Phys. Rev. Lett.* **2010**, 104, 136402.
- Schleck, R.; Nahas, Y.; Lobo, R. P. S. M.; Varignon, J.; Lepetit, M. B.; Nelson, C. S.; Moreira, R. L. *Phys. Rev. B* **2010**, 82, 054412.
- Jana, N. R.; Chen, Y.; Peng, X. *Chem. Mater.* **2004**, 16, 3931–3935.
- X-ray diffraction experiments conducted at 300 K yield 4.439 and 4.445 Å for the nanoparticles and bulk (see Supporting Information), respectively, where as neutron diffraction experiments conducted at 300 K yield 4.4438 ± 20 Å and 4.4467 ± 3 Å. There is some systematic variation in these numbers (particularly for the nanoparticles), depending on the choice of background. We consider these systems to be essentially isostructural within our sensitivity.
- Note that the theoretical calculated density of MnO single crystal is 5.366 g/cm³, and the actual densities of bulk powder and nanoparticle pellets are ~ 3.95 g/cm³ and ~ 2.54 g/cm³, respectively. Therefore, pellet densities are $\sim 74\%$ and $\sim 47\%$ of the single crystal density, respectively; we correct for this difference in our analysis.
- Homes, C. C.; Reedyk, M.; Cradles, D. A.; Timusk, T. *Appl. Opt.* **1993**, 32, 2976–2983.
- The presence of myristic acid can be verified by the typical spectral signatures near 1300 cm⁻¹ (lower right inset, Figure 3b), characteristic of organic stretching modes. Thus, the measured nanoparticle reflectance spectrum contains information on both the MnO nanoparticles and the capping ligands.
- Machefert, J. M.; Calvar, M. L.; Lenglet, M. *Surf. Interface Anal.* **1991**, 17, 137–142.
- Here, we account for the small portion of the incident light that is reflected by the organic capping layer, the larger part of the incident light that will pass through the capping ligand and be reflected by the MnO, and the multiple internal reflections and transmissions that subsequently take place.
- Wooten, F. *Optical Properties of Solids*; Academic Press: New York, 1972.
- We employed a constant low-frequency extrapolation, as appropriate for a semiconductor. Our high-frequency extrapolation was done as ω^{-2} .
- Sun, Q.-C.; Xu, X. S.; Vergara, L. I.; Rosentsveig, R.; Musfeldt, J. L. *Phys. Rev. B* **2009**, 79, 205405.
- Xu, X. S.; Sun, Q.-C.; Rosentsveig, S.; Musfeldt, J. L. *Phys. Rev. B* **2009**, 80, 014303.
- The bulk powder data has been corrected for surface scattering, and the nanoparticle data has been corrected for both surface scattering and the reflectance of the capping ligand.
- Cowley, R. A. *Rep. Prog. Phys.* **1968**, 31, 123–166.
- Eldridge, J. E.; Staal, P. R. *Phys. Rev. B* **1977**, 16, 4608.
- And also capping ligand effects for the nanoparticles.
- The error bars of $(\omega_p')^2$ and $\epsilon'(\infty)$ are $\pm 6.6 \times 10^4$ and ± 0.05 for the single crystal, and $\pm 3.7 \times 10^4$ and ± 0.06 for the nanoparticles. The error bars of Z_B^* , α , and Z^* are ± 0.07 , ± 0.2 , and ± 0.03 for the single crystal, and ± 0.05 , ± 0.3 , and ± 0.015 for the nanoparticles.
- The depolarization factor is $n = 1/3$ for a cubic system.
- Ashcroft, N. W.; Mermin, N. D. *Solid State Physics*; Thomson Learning: New York, 1976.
- Masenelli, B.; Nicolas, D.; Melinon, P. *Small* **2008**, 4, 1233–1239.
- The surface-to-volume ratios are 2.4×10^4 and 7.5×10^8 m⁻¹ for bulk powder and nanoparticles, respectively.
- Noguera, C. J. *Phys.: Condens. Matter* **2000**, 12, R367–R410.